Journal of Magnetic Resonance 205 (2010) 216–223

Contents lists available at ScienceDirect

Journal of Magnetic Resonance

journal homepage: www.elsevier.com/locate/jmr

Tailored low-power cross-polarization under fast magic-angle spinning

Jean-Philippe Demers, Vinesh Vijayan, Stefan Becker, Adam Lange *

Max Planck Institute for Biophysical Chemistry, Solid-state NMR, Göttingen 37077, Germany

ARTICLE INFO

Article history:
Received 19 March 2010
Available online 6 May 2010

Keywords:
Solid-state NMR
Fast magic-angle spinning
Cross-polarization
Amplitude modulation
Low-power pulse sequences
Bandwidth
MOD-CP
SOCP

ABSTRACT

High static magnetic fields and very fast magic-angle spinning (MAS) promise to improve resolution and sensitivity of solid-state NMR experiments. The fast MAS regime has permitted the development of low-power cross-polarization schemes, such as second-order cross-polarization (SOCP), which prevent heat deposition in the sample. Those schemes are however limited in bandwidth, as weak radio-frequency (RF) fields only cover a small chemical shift range for rare nuclei (e.g. ^{13}C). Another consideration is that the efficiency of cross-polarization is very sensitive to magnetization decay that occurs during the spin-lock pulse on the abundant nuclei (e.g. ^{1}H). Having characterized this decay in glutamine at 60 kHz MAS, we propose two complementary strategies to tailor cross-polarization to desired spectral regions at low RF power. In the case of multiple sites with small chemical shift dispersion, a larger bandwidth for SOCP is obtained by slightly increasing the RF power while avoiding recoupling conditions that lead to fast spin-lock decay. In the case of two spectral regions with large chemical shift offset, an extension of the existing low-power schemes, called MOD-CP, is introduced. It consists of a spin-lock on ^{1}H and an amplitude-modulated spin-lock on the rare nucleus. The range of excited chemical shifts is assessed by experimental excitation profiles and numerical simulation of an I_2S spin system. All SOCP-based schemes exhibit higher sensitivity than high-power CP schemes, as demonstrated on solid (glutamine) and semi-solid (hydrated, micro-crystalline ubiquitin) samples.

1. Introduction

The past decade has seen a tremendous development in the field of solid-state NMR [1,2]. Part of this development can be attributed to the widespread adoption of high static magnetic fields. High fields provide better sensitivity, since the improvement in signal-to-noise ratio (S/N) is roughly proportional to $B_0^{3/2}$. Furthermore, chemical shift dispersion directly scales with the field strength, which is beneficial for the resolution of crowded spectra. Similar to the progress provided by high B_0 fields, a recent wave of improvement in resolution and sensitivity has been brought about by the development of very fast MAS probe heads and pulse techniques. MAS frequencies of up to 67 kHz are now reached by rotors with an o.d. of 1.3 mm. As a consequence of the very fast rotation, chemical shift anisotropies are efficiently averaged and dipolar couplings are greatly reduced [3], resulting in narrow line-widths. The large decrease in sample volume reduces the sensitivity; this effect is partially compensated since the S/N per unit volume follows the inverse of the RF coil diameter [4,5]. Therefore, at equal MAS speed, the absolute S/N is roughly proportional to the rotor diameter.

At high static field, large chemical shift dispersions entail the generation of larger applied B_1 fields in order to excite the full spectral width of nuclei such as ^{13}C and ^{15}N. Strong radio-frequency (RF) irradiation can deposit a high amount of energy in the sample. The heat contributed can lead to irremediable alteration of the sample. This situation is particularly critical for the study of biological samples, which are fragile and often preserved in ionic buffers [6]. In fast MAS experiments, additional heating is caused by the friction of the MAS rotor with the surrounding gas, which can increase the temperature by about 60 K at 60 kHz MAS. To overcome the heating problem, one strategy is to reduce electric fields through modifications of the RF coil design [7–13]. A concurrent and complementary strategy is the development of pulse sequences requiring minimal amounts of irradiation power. This additionally mitigates the strain that strong RF generation imposes on the instrumentation. Substantial gains in sensitivity can further be obtained by combining low-power pulse sequences and fast MAS with shortening of the recycling delay. For instance, in the presence of paramagnetic nuclei, the ^{1}H longitudinal relaxation times are reduced, thus allowing fast acquisition [14–18].

Low-power alternatives compatible with very fast magic-angle spinning of the rotor have been recently introduced for many of the fundamental building blocks of solid-state NMR pulse

* Corresponding author. Address: Max Planck Institute for Biophysical Chemistry, Solid-state NMR, Am Faßberg 11, 37077 Göttingen, Germany. Fax: +49 551 201 2202.
E-mail address: adla@nmr.mpibpc.mpg.de (A. Lange).

1090-7807/$ - see front matter © 2010 Elsevier Inc. All rights reserved.
doi:10.1016/j.jmr.2010.04.019

sequences. This comprises proton hetero-nuclear decoupling (e.g. XiX [19–21], TPPM [22–24], PISSARRO [25]), mixing schemes (e.g. HORROR [26], ocHORROR [27], DREAM [21,28,29], RFDR [30–32], MIRROR [33], PARIS [34], PAR [35,36]), and cross-polarization [37,38]. Low-power cross-polarization schemes, such as band-selective ^{1}H–^{13}C cross-polarization [37], and second-order cross-polarization (SOCP) [38], are easily incorporated into multidimensional experiments. The band-selective ^{1}H–^{13}C CP was included in the low-power pulse sequence for CC-RFDR [17]. We have recently presented a set of low-power solid-state NMR experiments assembled based on SOCP, (NCA, N(CO)CX and CC), that are sufficient for protein resonance assignment under fast MAS, and which include sequential ^{15}N–^{13}C correlation [18]. SOCP is a second order recoupling experiment, part of the growing family that presently consists of PAIN-CP [39], PAR [35,36,40], MIRROR [33], RESORT [41] and SOCP.

An intrinsic limitation of the low-power CP schemes is their band-selective aspect, since a low-power irradiation cannot efficiently spin-lock the full range of chemical shifts for rare nuclei. In the current article, we present two strategies to alleviate this limitation. In case of multiple sites with small chemical shift dispersion, we employ SOCP with increased RF frequency. In case of regions with large chemical shift dispersion, low-power CP is employed with an amplitude modulation on the rare nucleus (the "S" spin) spin-lock pulse. This constitutes an extension of the present schemes which restores the high information content per spectrum that is found in broadband excitation while conserving the benefits of low-power solid-state NMR pulse sequences.

In order to select optimal conditions, we first characterized the decay of ^{1}H spin-locked magnetization as a function of RF-field strength and MAS frequency. The effect of amplitude modulation on cross-polarization is then analyzed through experimental and simulated excitation profiles. The efficiency of the cross-polarization schemes is demonstrated on solid (glutamine as a dry powder) and semi-solid (hydrated, micro-crystalline ubiquitin [42]) samples. Finally, SOCP with increased bandwidth is used to record an entirely low-power 2D ^{13}C–^{13}C correlation experiment on ubiquitin. The obtained spectrum contains correlations for complete amino acid spin systems, including carbonyl, aromatic and methyl carbons.

2. Materials and methods

2.1. Sample preparation

Uniformly [^{13}C, ^{15}N]-labeled ubiquitin was recombinantly expressed in *E. coli* and purified as previously described [42,43]. Micro-crystals were obtained by precipitating the sample with polyethylene glycol [44]. Approximately 1 mg of micro-crystalline protein was filled into a rotor of o.d. 1.3 mm. A 1.3-mm rotor was packed with 2.91 mg of uniformly [^{13}C, ^{15}N]-labeled L-glutamine purchased from Cambridge Isotope Laboratories (Cambridge, MA).

2.2. Solid-state NMR spectroscopy

Spectra were recorded at 18.8 T (800 MHz ^{1}H Larmor frequency) on a Bruker Avance III standard-bore spectrometer equipped with a 1.3-mm triple-resonance probe head (Bruker). Three MAS frequencies were used for the spin-lock experiments: 40.2, 49.9, and 60.0 kHz. All other experiments were performed at 60.0 kHz. The temperature of the ubiquitin sample was estimated to be +6.7 °C at a MAS frequency of 40 kHz, +17.0 °C at 50 kHz and +31.0 °C at 60 kHz. This estimate was obtained by comparison of the isotropic ^{1}H chemical shift of water at high-speed MAS to published chemical shifts [45]. For all experiments, the ^{1}H–^{13}C and ^{1}H–^{15}N dipolar couplings were decoupled during acquisition using 12 kHz of XiX decoupling on ^{1}H [19,20]. A recycling delay of 2 s was employed. Chemical shifts are reported in ppm from DSS, calibrated using adamantane as external reference [46]. CP-MAS spectra were acquired with 128 scans for ubiquitin (Fig. 4a,b and d) and 32 scans for glutamine (Figs. 4 and 6). The 2D ^{13}C–^{13}C DREAM spectrum was recorded with 250 t_1 points and 288 scans, for a total experimental time of 40 h. The maximum acquisition time was 6.2 ms in the t_1 and 14.4 ms in the t_2 dimension. Double-quantum ^{13}C–^{13}C mixing was accomplished by a tangential amplitude sweep [28,29] from ~25 to ~35 kHz during 5 ms.

2.3. Measurement of excitation profiles

Signal intensity was detected after a cross-polarization of 5 ms through a series of ^{1}H–^{15}N CP-MAS spectra of glutamine (Fig. 2). To record a complete profile, the ^{15}N carrier was swept from 102 kHz upfield to 102 kHz downfield of the resonances in steps of 750 Hz. The glutamine ^{15}N spectrum has two resonances corresponding to the side-chain amide and to the backbone amine at 111.1 ppm and 38.16 ppm, respectively. The homonuclear dipolar couplings between ^{15}N are considered to be insignificant, based on the large distance separation between two nitrogen atoms in the crystal structure (Refs. [47,48]). Hence, signals from both side-chain and backbone were combined in the analysis to increase *S*/*N*.

2.4. Quantum mechanical simulations

The simulated excitation profiles of ^{1}H–^{15}N CP in glutamine were obtained from a step-wise integration procedure of the Liouville–von Neumann equation within the numerical simulation routine GAMMA [49]. Neglecting scalar through-bond couplings, the relevant Hamiltonian in the Zeeman interaction frame contains ^{15}N isotropic chemical shift, dipolar couplings (^{1}H–^{1}H and ^{1}H–^{15}N) and RF irradiation on ^{1}H and ^{15}N (time-dependent in case of MOD-CP). Mimicking the situation in an NH_2 group, a proton-proton distance of 1.74 Å (corresponding dipolar coupling: 23.2 kHz) and proton-nitrogen distances of 1.05 Å (dipolar coupling: 10.5 kHz) were used. To obtain a complete excitation profile, simulations were carried out in steps of 375 Hz such that the ^{15}N isotropic chemical shift covered a range from –102 kHz to +102 kHz. The expectation value of spin-locked ^{15}N magnetization was averaged for all time points between 6 ms and 8 ms. Powder averaging involved 120 orientations. All simulated profiles were adjusted with a single, global scaling factor in order to be compared with experimental profiles. This global scaling factor was found by least-squares fitting of simulated to observed signal intensities.

3. Results and discussion

3.1. Characteristics of spin-locked magnetization

A ubiquitous building block in solid-state NMR pulse sequences is the spin-lock RF pulse. Magnetization is preserved along a given axis in the rotating frame by the application of an external field $\vec{B}_1$ parallel to this axis. If the RF field is sufficiently strong, then dephasing due to dipolar couplings and chemical shifts is small or negligible. Magnetization can thus be stored for relatively long periods, limited only by the spin–lattice relaxation in the rotating frame with a time constant $T_{1\rho}$. However, at specific amplitudes of the RF field, some spin interactions are reintroduced because of the interference between RF irradiation and MAS. These

recoupling conditions lead to dephasing and loss of stored magnetization.

We studied the dependence of recoupling conditions on MAS frequency, performing the spin-lock experiments at three different MAS frequencies: 40 kHz, 50 kHz, and 60 kHz (Fig. 1). The decay of ^{1}H (the "I" spin) magnetization was monitored by applying a spin-lock for 2.5 ms in glutamine, with nutation frequencies ν_1^H ranging from 0 to 3 × ν_{MAS}. The remaining magnetization was transferred for detection to the nearest ^{13}C nucleus through a high-power ZQ CP. The signal presented in Fig. 1 represents the addition of intensities from all five ^{13}C resonances of glutamine. The three intensity curves at different MAS were individually normalized against a control experiment in which the ^{1}H spin-lock period was omitted (i.e. a normal ZQ CP experiment without a spin-lock between ^{1}H 90° pulse and CP).

As previously described [38], spin-locked proton magnetization decays rapidly when the ratio of nutation frequency to MAS frequency, $\kappa = \nu_1^H/\nu_{MAS}$, is around $\kappa = \frac{1}{4}, \frac{1}{3}, \frac{1}{2}, 1, \frac{3}{2}$, or 2. Those conditions are indicated in Fig. 1 by asterisks. At $\kappa = \frac{1}{2}$, the HORROR condition [26], homonuclear dipolar couplings are recoupled; at the $\kappa = 1$ rotary resonance condition, chemical shift anisotropies as well as homonuclear and hetero-nuclear dipolar couplings are recoupled; while the $\kappa = 2$ rotary resonance condition recouples chemical shift anisotropies and hetero-nuclear dipolar couplings. The $\kappa = \frac{1}{4}, \frac{1}{3}$, and $\frac{3}{2}$ conditions can be understood in terms of higher-order perturbation theory [38,50].

Two inferences can be made as the MAS frequency increases. First, the overall magnetization decay is slower at high MAS, for all nutation frequencies with ratio $\kappa < 2$. Second, the range of RF-field frequencies (in Hz) affected around the $\kappa = \frac{1}{2}$ and $\kappa = 1$ conditions becomes considerably narrower at high MAS. The narrowing of the $\kappa = \frac{1}{2}$ and $\kappa = 1$ conditions is consistent with the interpretation that, while CSA and hetero-nuclear couplings are efficiently averaged out at 40 kHz of MAS, the averaging of proton homonuclear couplings benefits from further increase in the MAS frequency. Nicely, at 60 kHz MAS, we can find a band of frequencies below the $\kappa = \frac{1}{4}$ ratio which very effectively conserves the initial magnetization. After 2.5 ms of spin-lock, more than 95% of the magnetization is preserved for nutation frequencies between 7 kHz and 14 kHz. Other regions of low decay can be found in the following intervals: $\frac{1}{4} < \kappa < \frac{1}{3}$, $\frac{1}{2} < \kappa < 1$, $1 < \kappa < \frac{3}{2}$, $\frac{3}{2} < \kappa < 2$, $\kappa > 2$. At low MAS, however, only frequencies above the $\kappa = 2$ condition efficiently prevent rapid magnetization decay.

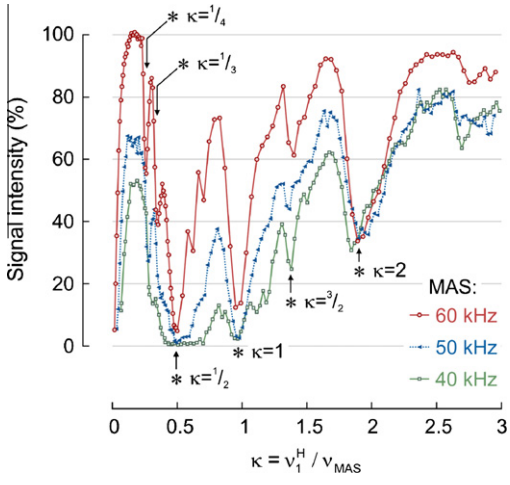

Fig. 1. Proton spin-lock efficiency as a function of RF-field strength ν_1^H and MAS frequency ν_{MAS}. Signal intensity is detected indirectly on ^{13}C after 2.5 ms of ^{1}H spin-lock. Spin-lock efficiency is measured at three different MAS frequencies: 40 kHz (green squares), 50 kHz (blue triangles), and 60 kHz (red circles). Asterisks indicate recoupling conditions that lead to rapid magnetization decay, near the ratios $\kappa = \{\frac{1}{4}, \frac{1}{3}, \frac{1}{2}, 1, \frac{3}{2}, 2\}$. (For interpretation of the references to colour in this figure legend, the reader is referred to the web version of this article.)

3.2. Second-order cross-polarization with increased bandwidth

Thus far, two cross-polarization schemes at low RF power and high MAS have been proposed. Under magic-angle spinning, cross-polarization is obtained when the effective nutation frequencies of the rare and abundant spins match the Hartmann-Hahn condition (Eq. (1)), see Refs. [51–54]. The addition (+) and difference (−) conditions correspond to double-quantum (DQ) and zero-quantum (ZQ) transfer, respectively.

$$\left|\nu_1^S \pm \nu_1^I\right| = n \cdot \nu_{MAS}, \quad n = \{0, 1, 2\} \tag{1}$$

The band-selective ^{1}H–^{13}C CP scheme [17,37] employs the $n = 1$ DQ condition. The proton spin-lock frequency is set between the $\kappa = \frac{1}{2}$ and $\kappa = 1$ ratio, at $\nu_1^H = \nu_{MAS} - \nu_1^C$, such that a low-power pulse can be used to spin-lock rare nuclei. In second-order cross-polarization (SOCP) [38], the I and S spin-lock frequencies are matched at the $n = 0$ Hartmann–Hahn condition, $\nu_1^I = \nu_1^S$. Magnetization transfer occurs predominantly through second-order cross-terms between homonuclear I–I and hetero-nuclear I–S dipolar couplings. SOCP allows the use of low-power RF for both nuclei, such that the proton spin-lock frequency is set below the $\kappa = \frac{1}{4}$ condition.

It should be noted that extending the bandwidth of SOCP is easily achieved by increasing the RF-field strength for both I and S nuclei while preserving $n = 0$ Hartmann–Hahn matching. The efficiency of the SOCP transfer deteriorates when ν_1^H approaches the $\kappa = \frac{1}{4}$ recoupling condition. However, the fast decay of spin-locked ^{1}H magnetization is avoided when the nutation frequency is carefully selected between the $\kappa = \frac{1}{4}$ and $\kappa = \frac{1}{3}$ ratios. Past the $\kappa = \frac{1}{3}$ ratio however, this approach is not advisable since recoupling conditions are encountered and power deposition in the sample increases with the square of the applied frequency. Increasing the bandwidth of SOCP is best suited when the chemical shift dispersion is small in comparison to the MAS frequency, which is most likely the case for moderate static fields and fast MAS, e.g. $B_0 \leqslant 14.1$ T (600 MHz ^{1}H Larmor frequency) and 60 kHz MAS.

3.3. Amplitude-modulated second-order cross-polarization (MOD-CP)

For higher static fields and very large chemical shift offsets, the SOCP with increased bandwidth approach is not appropriate and an alternative has to be sought. Pulses with a cyclical amplitude modulation are commonly employed for the selective excitation of two resonances [55–57]. A cross-polarization scheme with cosine or sine amplitude modulation has already been presented in solution-state NMR [58]. We thus considered the use of cosine amplitude modulation in combination with low-power CP in order to transfer polarization to multiple regions separated by a large chemical shift offset.

An applied RF pulse is described by a field strength B_1 (T) and a reference transmitter frequency ν_{ref} (Hz). By multiplying this general pulse with a cosine modulation of frequency ν_{mod} (Hz), we obtain (Eq. (2)):

$$\begin{aligned}\vec{B}_1^{mod} &= \vec{B}_{[B_1;\nu_{ref}]} \cdot \cos(2\pi\nu_{mod}t) \\ &= B_1 \cdot \left[\cos(2\pi\nu_{ref}t) \cdot \cos(2\pi\nu_{mod}t) \cdot \vec{e}_x + \sin(2\pi\nu_{ref}t) \right. \\ &\quad \left. \cdot \cos(2\pi\nu_{mod}t) \cdot \vec{e}_y\right]\end{aligned} \tag{2}$$

The effect of the modulation results from the product-to-sum trigonometric identity. It can be seen that this is equivalent to irradiation with two fields of half the strength (Eq. (3)). Therefore, in

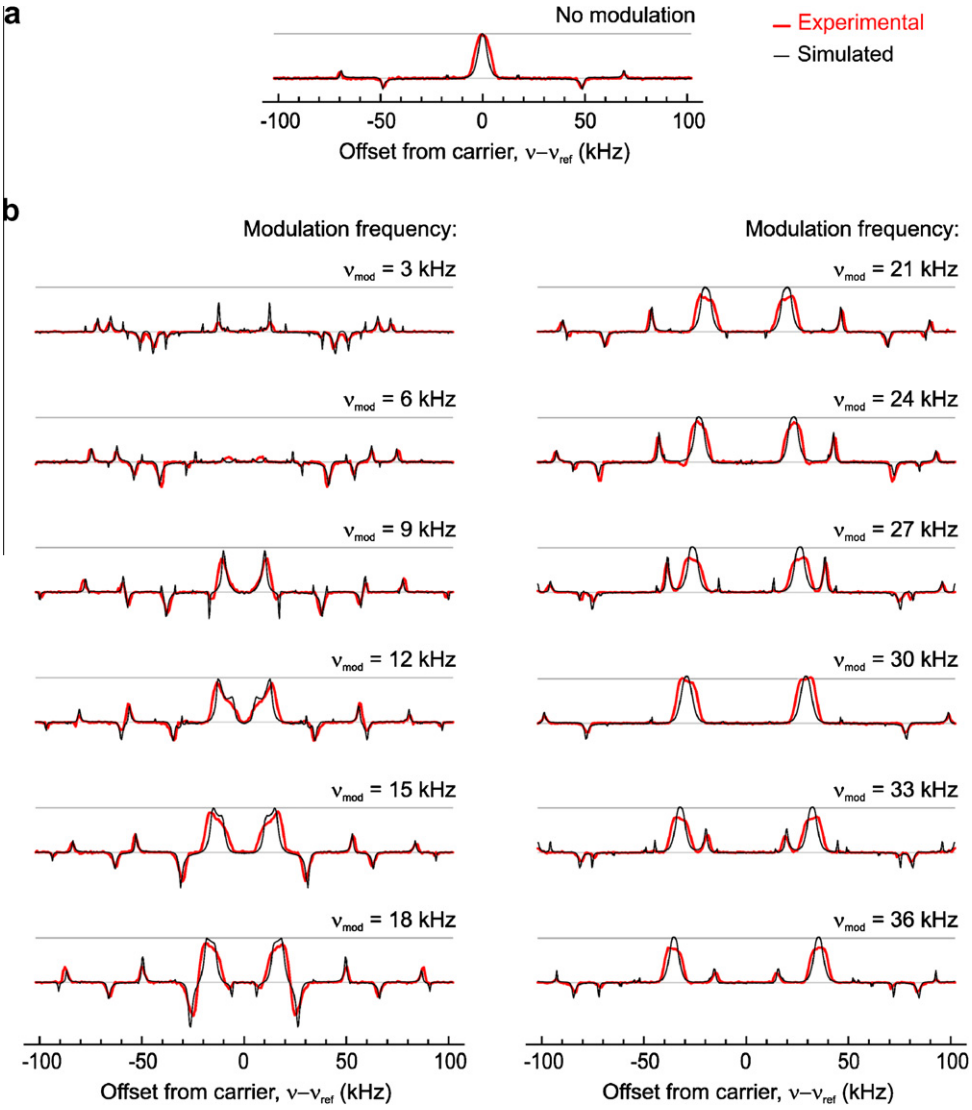

Fig. 2. Excitation profiles for SOCP and MOD-CP. For the experimental profiles (red), the signal intensity is measured on the ^{15}N resonances of glutamine after 5 ms of cross-polarization. Numerical simulations of the excitation profiles are shown in black. (a) SOCP, with $\nu_1^H = \nu_1^N = 10$ kHz. (b) MOD-CP, with $\nu_1^H = 10$ kHz, $\nu_1^N = 20$ kHz, and modulation frequencies ranging from 3 kHz to 36 kHz. Above 9 kHz of modulation frequency, two bands of intense positive transfer are observed at offsets of $-\nu_{mod}$ and $+\nu_{mod}$. (For interpretation of the references to colour in this figure legend, the reader is referred to the web version of this article.)

order to preserve the properties of the original pulse but transmit it simultaneously at two different offsets, the field strength has to be doubled.

$$\begin{aligned}\vec{B}_1^{mod} &= B_1 \cdot \left(\frac{1}{2}\left[\cos 2\pi(\nu_{ref} - \nu_{mod})t + \cos 2\pi(\nu_{ref} + \nu_{mod})t\right]\vec{e}_x \right.\\ &\left. + \frac{1}{2}\left[\sin 2\pi(\nu_{ref} - \nu_{mod})t + \sin 2\pi(\nu_{ref} + \nu_{mod})t\right]\vec{e}_y\right)\\ &= \vec{B}_{\left[\frac{1}{2}B_1;\nu_{ref}-\nu_{mod}\right]} + \vec{B}_{\left[\frac{1}{2}B_1;\nu_{ref}+\nu_{mod}\right]} \end{aligned} \quad (3)$$

MOD-CP is achieved by application of a spin-lock pulse on ^{1}H and an amplitude-modulated spin-lock pulse on the S spin (Fig. 4c). For two sites of interest, with isotropic chemical shifts δ_A and δ_B (ppm), the frequency of the amplitude modulation (in Hz) is $\nu_{mod} = \frac{1}{2}\cdot|\delta_A - \delta_B|\cdot\nu_{Larmor}$. The reference transmitter position for the S spin (in ppm) is set to the middle frequency between the two sites: $\Omega_{ref} = \frac{1}{2}\cdot|\delta_A + \delta_B|$. Compared to the regular SOCP, the applied field strength (B_1) for the rare spin is doubled. The original field strength applied on ^{1}H and carrier position are preserved. Following from (Eq. (3)), $n = 0$ Hartmann–Hahn matching is established at resonance frequencies $\nu_{ref} - \nu_{mod}$ and $\nu_{ref} + \nu_{mod}$. Additionally, the final phase for each excitation band can be controlled independently [56,59].

Excitation profiles (Fig. 2) confirm that the bandwidth and intensity of transfer remain constant for large modulation frequencies, $\nu_{mod} > \frac{1}{2}\nu_1^S$. From the experimental profiles, one can conclude that MOD-CP is a suitable method for the excitation of regions with large chemical shift separation. All features of the experimental profiles could be well reproduced by profiles simulated numerically within the GAMMA spin-simulation environment [49]. We considered an I_2S spin system as in an NH_2 group with two ^{1}H–^{15}N dipolar couplings and one ^{1}H–^{1}H dipolar coupling, as explained in more detail in the experimental section. Two bands of intense positive transfer are found at offsets of $-\nu_{mod}$ and $+\nu_{mod}$ relative to the carrier frequency, corresponding to on-resonance $n = 0$ Hartmann–Hahn matching (Fig. 3). Other transfer conditions, with $n > 0$, are also matched off-resonance; this is seen in the excitation profile as positive (ZQ) or negative (DQ) transfer bands far away from the carrier position. The signal intensity for those bands is however reduced since the axis of the effective RF field is tilted away from the transverse plane.

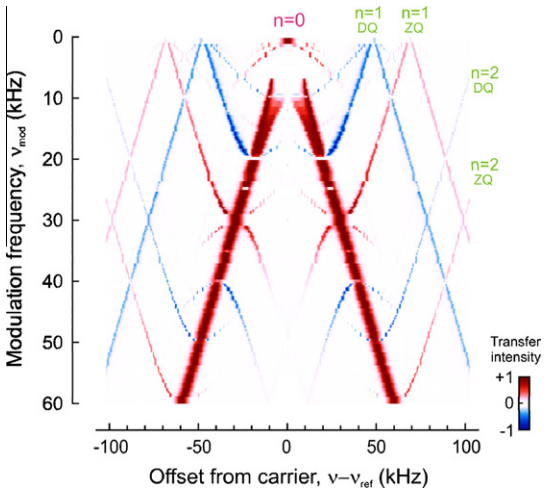

Fig. 3. Simulation of magnetization transfer as a function of carrier offset and MOD-CP modulation frequency. Positive transfer is indicated in red and negative transfer in blue. The dominant transfer at offsets of $-\nu_{mod}$ and $+\nu_{mod}$ corresponds to an on-resonance $n = 0$ Hartmann–Hahn condition. Magnetization transfer occurs as well off-resonance at sideband Hartmann–Hahn conditions ($n = 1$, $n = 2$), albeit with lesser intensity. Numerical simulations were carried out within the GAMMA spin-simulation environment considering an NH_2 spin system.

Table 1
Experimental parameters for cross-polarization at 60 kHz MAS and 800 MHz ^{1}H Larmor frequency.

Sample	$\overline{\nu_1}$ (kHz)	τ_{cp} (ms)	Region excited	^{13}C Ω_{ref} (ppm)	Notes
Double-quantum (n=2) CP					
Ubiquitin	^{1}H 85	1.3	Broadband	100	100–80% ramp on ^{1}H pulse
	^{13}C 35				
Zero-quantum (n=1) CP					
Glutamine	^{1}H 100	0.8	Broadband	100	100–80% ramp on ^{1}H pulse
	^{13}C 40				
Second-order (n=0) CP					
Ubiquitin	^{1}H 9	2.5	C′	175	
	^{13}C 9		C_α	56	
			C_β	28	
Glutamine	^{1}H 10	5.0	C′	177.5	
	^{13}C 10		C_α/C_β	42.5	
SOCP with increased bandwidth					
Ubiquitin	^{1}H 19	1.4	$C_\alpha + C_\beta$	40	
	^{13}C 19				
Amplitude-modulated SOCP (MOD-CP)					
Ubiquitin	^{1}H 9		C′ + C_α	115.5	11.9 kHz modulation on ^{13}C pulse
	^{13}C 18	2.5	C′ + C_β	101.5	14.7 kHz modulation on ^{13}C pulse
Glutamine	^{1}H 10	5.0	C′ + C_α/C_β	110	13.5 kHz modulation on ^{13}C pulse
	^{13}C 20				
Amplitude-modulated band-selective CP					
Glutamine	^{1}H 50	3.0	C′ + C_α/C_β	110	13.5 kHz modulation on ^{13}C pulse
	^{13}C 20				

$\overline{\nu_1}$: mean frequency of the RF-field.
τ_{CP}: contact time.
Ω_{ref}: transmitter frequency.

Simulation and experiments demonstrate the consistent performance of MOD-CP over a wide range of modulation frequencies. A notable limitation is that the modulation frequency must be sufficiently large, $\nu_{mod} > \frac{1}{2}\nu_1^S$ (see Fig. 3). Below this threshold, the two excitation bands come close together such that the rare nuclei experience two B_1 fields. The two effective fields have a slightly different axis of nutation, resulting in dephasing of magnetization

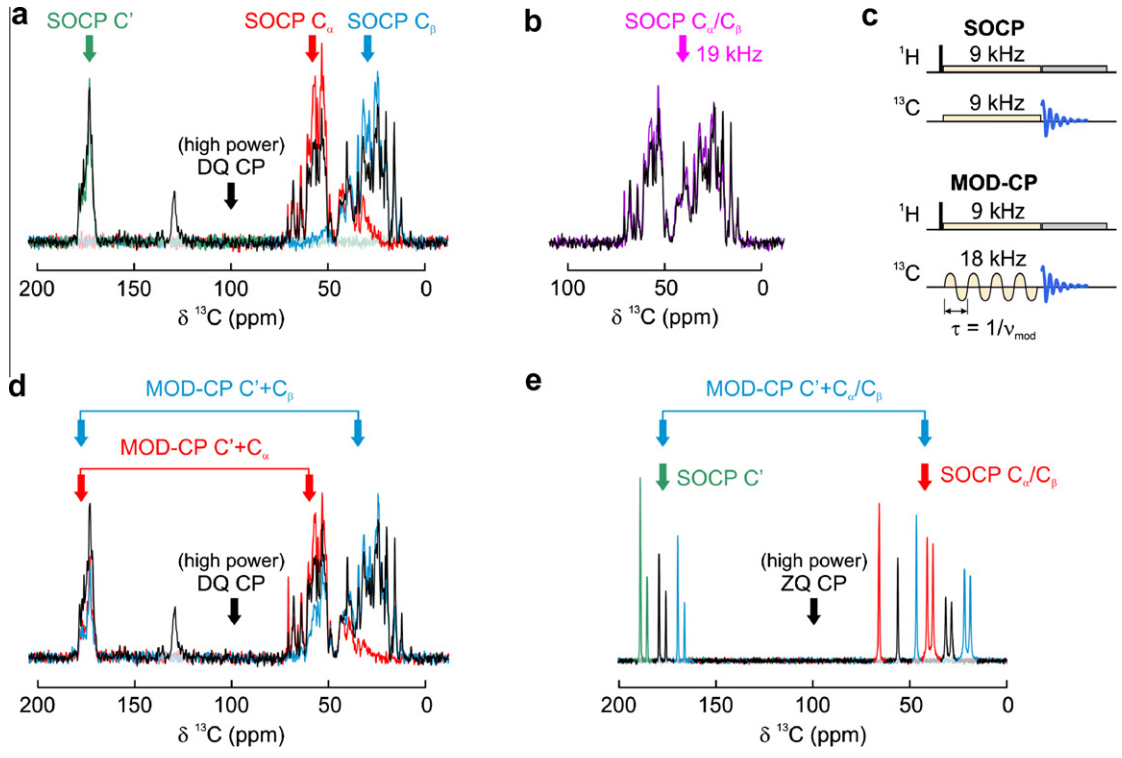

Fig. 4. Comparison of cross-polarization efficiencies. (a) ^{13}C CP-MAS spectra of micro-crystalline ubiquitin utilizing high-power DQ CP (black), or regular SOCP, $\nu_1^H = \nu_1^C = 9$ kHz, on the C′ (green), C_α (red), or C_β region (blue). The ^{13}C carrier positions are indicated by arrows. (b) SOCP on the aliphatic region with $\nu_1^H = \nu_1^C = 19$ kHz (pink) is compared to high-power CP (black, as in a). (c) Pulse schemes for SOCP (top) and MOD-CP (bottom). In MOD-CP, a cosine amplitude modulation is applied to the ^{13}C spin-lock pulse, and the frequency ν_1^C is doubled to excite both ^{13}C regions. (d) MOD-CP can excite both the C′ and C_α regions (red), or both the C′ and C_β regions (blue). (e) ^{13}C CP-MAS spectra of glutamine using high-power ZQ CP (black), MOD-CP (blue), and SOCP on the C′ (green) or C_α (red) regions. Spectra are shifted from the high-power ZQ CP for better visibility.

rather than spin-lock. In this case, SOCP with increased bandwidth can be employed to complement MOD-CP.

3.4. Optimal cross-polarization conditions

The efficiency of three cross-polarization schemes was assessed: (i) high-power CP, (ii) SOCP, and (iii) MOD-CP. We acquired ^{13}C CP-MAS spectra in order to compare the three schemes in terms of bandwidth and sensitivity (Fig. 4). The optimized experimental parameters for cross-polarization are summarized in Table 1.

The conditions for broadband transfer at high power were optimized for maximal overall signal intensity. A linear amplitude sweep is used on the ^{1}H spin-lock pulse to ensure that the transfer is resilient to Hartmann-Hahn mismatch [60]. In ubiquitin, the best cross-polarization was obtained at the DQ $n = 2$ condition, with $\overline{\nu_1^H} = 85$ kHz (mean frequency), $\nu_1^C = 35$ kHz during 1.3 ms. In glutamine, best transfer was achieved at the ZQ $n = 1$ condition, with nutation frequencies of $\overline{\nu_1^H} = 100$ kHz, $\nu_1^C = 40$ kHz, and a contact time of 0.8 ms.

Much lower nutation frequencies are employed for SOCP: 2.5 ms of spin-lock at 9 kHz for ubiquitin, and 5 ms at 10 kHz for glutamine. The higher sensitivity of regular SOCP compared to high-power CP is readily apparent (Fig. 4a and e), and is explained by various reasons. An intrinsic feature of SOCP is that the initial magnetization can originate from protons not directly coupled to the S spin. In the thermodynamic limit, a narrow ^{13}C bandwidth also contributes to enhanced signal, since magnetization is shared among a lesser number of carbons. Matching at the $n = 0$ condition makes the SOCP scheme less sensitive to RF field inhomogeneities and thermal drift of the amplifiers [38]. Finally, the ^{1}H spin-lock is most efficient at low RF power, as previously discussed.

The two proposed strategies to extend the ^{13}C bandwidth are complementary and suited to different situations. The first strategy, consisting of SOCP transfer with increased RF power levels, is appropriate for small chemical shift dispersion. For instance, by selecting the ^{1}H and ^{13}C nutation frequency between the $\kappa = \frac{1}{4}$ and $\kappa = \frac{1}{3}$ ratios, one can excite the full ^{13}C aliphatic region in a spectrometer operating at 18.8 T (800 MHz ^{1}H Larmor frequency). This would not be possible with MOD-CP; at 18.8 T, the C_α and C_β regions have a separation of 5.6 kHz, which is lower than the desired nutation frequency, $\frac{1}{2}\nu_1^C \approx 9$ kHz. The second strategy, MOD-CP, is best suited for two regions with a large chemical shift offset. The excitation of the full ^{13}C aliphatic region at 60 kHz MAS, from about 5 to 75 ppm, is illustrated for uniformly labeled ubiquitin by the spectrum of SOCP with increased bandwidth (Fig. 4b). Nutation frequencies of 19 kHz are used during 1.4 ms.

We acquired a 2D ^{13}C–^{13}C DREAM spectrum (Fig. 5) employing SOCP with $\nu_1^H = \nu_1^C = 19$ kHz as the initial cross-polarization step and compared it to a similar spectrum employing SOCP with $\nu_1^H = \nu_1^C = 9$ kHz [18]. All cross-peaks from the regular SOCP spectrum appear at the same position in the increased-bandwidth SOCP spectrum. In addition, the latter spectrum contains many cross-peaks which are absent in the regular SOCP spectrum. This offers

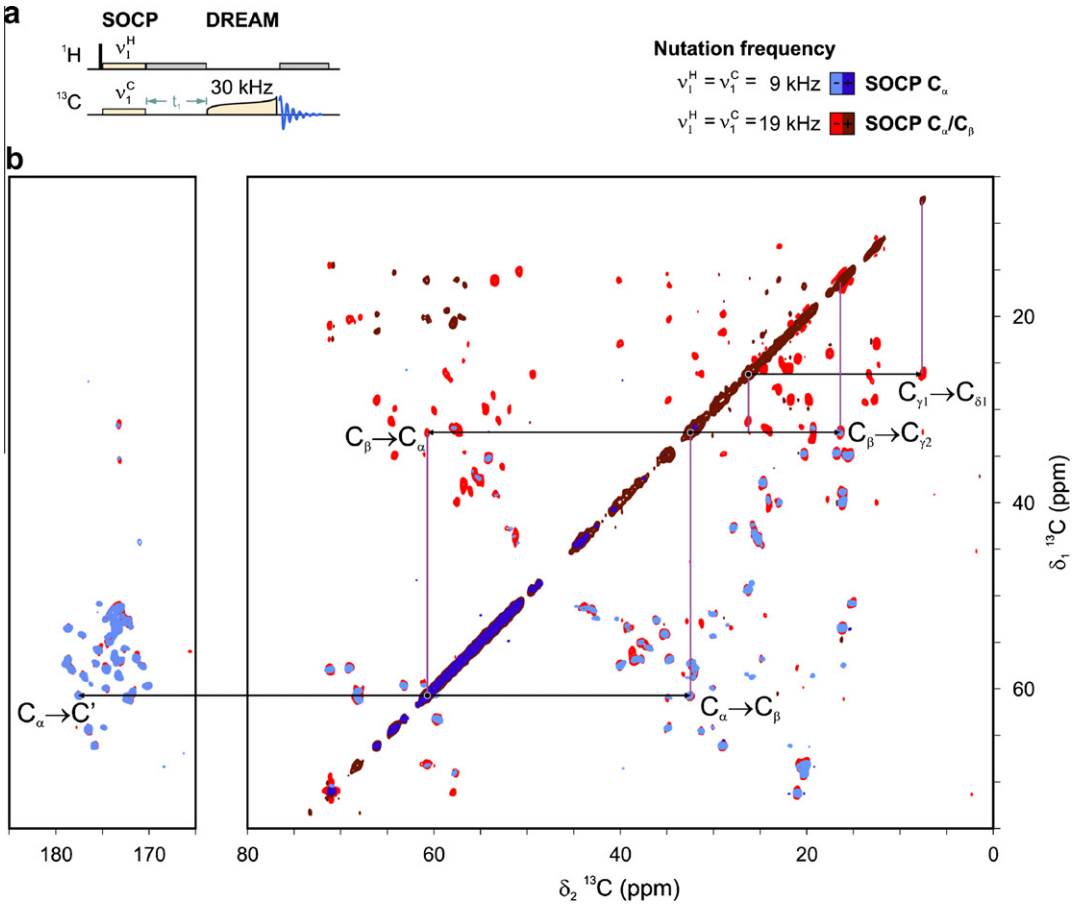

Fig. 5. ^{13}C–^{13}C DREAM correlation spectrum of micro-crystalline ubiquitin. (a) SOCP is used for the initial polarization transfer from ^{1}H to ^{13}C. In one case, regular SOCP is used with the ^{13}C carrier at 56 ppm to first excite the C_α region. In the other case, SOCP with increased bandwidth is employed with the ^{13}C carrier at 40 ppm to excite the full aliphatic region. A tangential amplitude sweep applied on ^{13}C allows dipolar recoupling of adjacent carbons. (b) The 2D spectra resulting from those two SOCP conditions are overlayed. Positive and negative peaks are indicated in dark and light blue, respectively, for regular SOCP (spectrum reproduced from [18]); and in dark and light red for SOCP with increased bandwidth. For illustrative purposes, cross-peaks enabling the assignment of the Ile23 spin system are indicated.

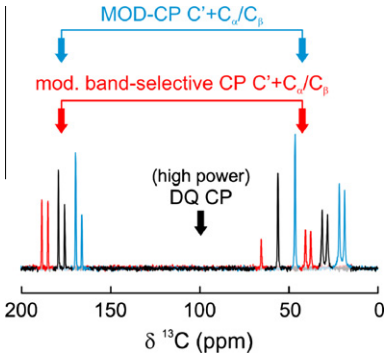

Fig. 6. The amplitude modulation approach can be used in combination with various CP schemes. In this case, CP-MAS spectra of glutamine were acquired using either an amplitude-modulated band-selective ^{1}H–^{13}C CP (red, $\nu_1^H = 50$ kHz, $\nu_1^C = 20$ kHz, 3 ms), or an amplitude-modulated SOCP (blue, $\nu_1^H = 10$ kHz, $\nu_1^C = 20$ kHz, 5 ms). The spectra are compared to a high-power ZQ CP (black, $\nu_1^H = 100$ kHz, $\nu_1^C = 40$ kHz, 0.8 ms) and were shifted for better visibility.

the possibility of identifying all ^{13}C–^{13}C correlations within the spin system of an amino acid. The assignment of ^{13}C resonances from an isoleucine residue (Ile23), from the carbonyl to the methyl carbons, is highlighted in Fig. 5.

MOD-CP is demonstrated on ubiquitin (Fig. 4d) and glutamine (Fig. 4e). In ubiquitin, magnetization is transferred simultaneously to the C′ and C_α regions by applying the ^{13}C pulse at 115.5 ppm with a modulation of 11.9 kHz. Alternatively, the C′ and C_β regions are excited with the ^{13}C spin-lock pulse at 101.5 ppm and an amplitude modulation of 14.7 kHz. In both cases, RF-field frequencies are $\nu_1^H = 9$ kHz and $\nu_1^C = 18$ kHz, with a contact time of 2.5 ms. In glutamine, MOD-CP excites all five ^{13}C resonances when the ^{13}C spin-lock pulse is applied at 110 ppm with a modulation of 13.5 kHz. RF-field frequencies are $\nu_1^H = 10$ kHz and $\nu_1^C = 20$ kHz, with a contact time of 5 ms. With the exception of C′, which is slightly reduced, all ^{13}C resonances exhibit greater transfer intensity with MOD-CP and increased-bandwidth SOCP than with the high-power CP schemes.

Under particular circumstances, a given cross-polarization scheme might be advantageous compared to another one. Thus, it was verified that the amplitude modulation approach can be used in combination with various CP schemes. We used band-selective ^{1}H–^{13}C CP (Ref. [37]) in combination with a modulated ^{13}C pulse to simultaneously excite C′ and C_α/C_β (Fig. 6). The band-selective ^{1}H–^{13}C CP could likely be preferred in cases where the site of interest is scarcely protonated, since SOCP requires at least two protons coupled to each other with at least one of them coupled to the S spin. Indeed, band-selective ^{1}H–^{13}C CP works very well for transfer to carbonyls. In this study, SOCP was preferred because it is currently the CP scheme with the lowest power requirement.

4. Conclusion

Three variations of the SOCP scheme are now available for low-power pulse sequences at fast MAS: regular SOCP, SOCP with increased bandwidth, and MOD-CP. Our results show that all SOCP-based schemes are more efficient than high-power CP for their respective bandwidth, while requiring less RF power. Regular SOCP still offers the highest sensitivity albeit at the cost of low bandwidth. MOD-CP and increased-bandwidth SOCP allow the precise selection of chemical shifts for rare nuclei, extending the spectral editing capability of SOCP. This can particularly benefit experiments containing multiple ^{1}H CP steps, for instance CHHC and NHHC [61,62]. In this study, we recorded a 2D ^{13}C–^{13}C correlation spectrum that contains ^{13}C–^{13}C correlations for complete amino acid spin systems, including carbonyl, aromatic and methyl carbons, as a demonstration of SOCP with increased bandwidth. MOD-CP supports a wide range of modulation frequencies (>36 kHz), which is advantageous for the study of biomolecules. As proton homonuclear decoupling techniques improve [63–67], MOD-CP could become useful for low-power hetero-nuclear correlation (HETCOR) experiments.

In summary, the proposed schemes are able to tailor cross-polarization to desired spectral regions with high efficiency and low RF power. The low power requirements of these schemes prevent RF heating and alteration of the sample. The deleterious effects of heating on spectral quality as well as the strain on the instrument are consequently reduced. In addition, sensitivity enhancement by fast acquisition and decreased recycle time resulting from paramagnetic relaxation is only feasible if entirely low-power sequences are available. Those factors advocate for a general use of SOCP-based schemes as an alternative to high-power CP. We therefore expect that their use will be beneficial for the investigation of biomolecular solids at high resolution and sensitivity.

Many other nuclei, such as ^{31}P, ^{15}N, ^{29}Si, and ^{19}F, cover a large range of isotropic chemical shifts [68]. Along with developments in probe head technology, the study of materials containing those nuclei can also benefit from fast MAS and SOCP-based transfer schemes.

Acknowledgments

We thank Prof. Beat Meier, Dr. Matthias Ernst and Dr. Robert Schneider for discussions, Brigitta Angerstein for expert technical assistance, and Karin Giller for sample preparation. Furthermore, we are grateful to Prof. Christian Griesinger for generous support of our work.

We thank the Max Planck Society and the Deutsche Forschungsgemeinschaft (Emmy Noether Fellowship to A.L.) as well as the Natural Sciences and Engineering Research Council of Canada (postgraduate scholarship to J.P.D.) for financial support.

References

[1] A. Lesage, Recent advances in solid-state NMR spectroscopy of spin I = 1/2 nuclei, Phys. Chem. Chem. Phys. 11 (2009) 6876–6891.
[2] A. McDermott, Structure and dynamics of membrane proteins by magic angle spinning solid-state NMR, Annu. Rev. Biophys. 38 (2009) 385–403.
[3] M. Ernst, A. Samoson, B.H. Meier, Low-power decoupling in fast magic-angle spinning NMR, Chem. Phys. Lett. 348 (2001) 293–302.
[4] T.L. Peck, R.L. Magin, P.C. Lauterbur, Design and analysis of microcoils for NMR microscopy, J. Magn. Reson., Ser. B 108 (1995) 114–124.
[5] M. Ernst, A. Detken, A. Bockmann, B.H. Meier, NMR spectra of a microcrystalline protein at 30 kHz MAS, J. Am. Chem. Soc. 125 (2003) 15807–15810.
[6] J.B.D. de Lacaillerie, B. Jarry, O. Pascui, D. Reichert, "Cooking the sample": radiofrequency induced heating during solid-state NMR experiments, Solid State Nucl. Magn. Reson. 28 (2005) 225–232.
[7] J.A. Stringer, C.E. Bronnimann, C.G. Mullen, D.H.H. Zhou, S.A. Stellfox, Y. Li, E.H. Williams, C.M. Rienstra, Reduction of RF-induced sample heating with a scroll coil resonator structure for solid-state NMR probes, J. Magn. Reson. 173 (2005) 40–48.
[8] F.D. Doty, J. Kulkarni, C. Turner, G. Entzminger, A. Bielecki, Using a cross-coil to reduce RF heating by an order of magnitude in triple-resonance multinuclear MAS at high fields, J. Magn. Reson. 182 (2006) 239–253.
[9] P.L. Gor'kov, E.Y. Chekmenev, C.G. Li, M. Cotten, J.J. Buffy, N.J. Traaseth, G. Veglia, W.W. Brey, Using low-E resonators to reduce RF heating in biological samples for static solid-state NMR up to 900 MHz, J. Magn. Reson. 185 (2007) 77–93.
[10] A. Krahn, U. Priller, L. Emsley, F. Engelke, Resonator with reduced sample heating and increased homogeneity for solid-state NMR, J. Magn. Reson. 191 (2008) 78–92.
[11] C.H. Wu, C.V. Grant, G.A. Cook, S.H. Park, S.J. Opella, A strip-shield improves the efficiency of a solenoid coil in probes for high-field solid-state NMR of lossy biological samples, J. Magn. Reson. 200 (2009) 74–80.

[12] C.V. Grant, Y. Yang, M. Glibowicka, C.H. Wu, S.H. Park, C.M. Deber, S.J. Opella, A modified Alderman–Grant coil makes possible an efficient cross-coil probe for high field solid-state NMR of lossy biological samples, J. Magn. Reson. 201 (2009) 87–92.
[13] S.A. McNeill, P.L. Gor'kov, K. Shetty, W.W. Brey, J.R. Long, A low-E magic angle spinning probe for biological solid state NMR at 750 MHz, J. Magn. Reson. 197 (2009) 135–144.
[14] R. Linser, V. Chevelkov, A. Diehl, B. Reif, Sensitivity enhancement using paramagnetic relaxation in MAS solid-state NMR of perdeuterated proteins, J. Magn. Reson. 189 (2007) 209–216.
[15] N.P. Wickramasinghe, M.A. Shaibat, C.R. Jones, L.B. Casabianca, A.C. de Dios, J.S. Harwood, Y. Ishii, Progress in ^{13}C and ^{1}H solid-state nuclear magnetic resonance for paramagnetic systems under very fast magic angle spinning, J. Chem. Phys. 128 (2008) 052210.
[16] N.P. Wickramasinghe, S. Parthasarathy, C.R. Jones, C. Bhardwaj, F. Long, M. Kotecha, S. Mehboob, L.W.M. Fung, J. Past, A. Samoson, Y. Ishii, Nanomole-scale protein solid-state NMR by breaking intrinsic $^{1}HT^{1}$ boundaries, Nature Meth. 6 (2009) 215–218.
[17] S. Laage, J.R. Sachleben, S. Steuernagel, R. Pierattelli, G. Pintacuda, L. Emsley, Fast acquisition of multi-dimensional spectra in solid-state NMR enabled by ultra-fast MAS, J. Magn. Reson. 196 (2009) 133–141.
[18] V. Vijayan, J.P. Demers, J. Biernat, E. Mandelkow, S. Becker, A. Lange, Low-power solid-state NMR experiments for resonance assignment under fast magic-angle spinning, ChemPhysChem 10 (2009) 2205–2208.
[19] A. Detken, E.H. Hardy, M. Ernst, B.H. Meier, Simple and efficient decoupling in magic-angle spinning solid-state NMR: the XiX scheme, Chem. Phys. Lett. 356 (2002) 298–304.
[20] M. Ernst, A. Samoson, B.H. Meier, Low-power XiX decoupling in MAS NMR experiments, J. Magn. Reson. 163 (2003) 332–339.
[21] M. Ernst, M.A. Meier, T. Tuherm, A. Samoson, B.H. Meier, Low-power high-resolution solid-state NMR of peptides and proteins, J. Am. Chem. Soc. 126 (2004) 4764–4765.
[22] A.E. Bennett, C.M. Rienstra, M. Auger, K.V. Lakshmi, R.G. Griffin, Heteronuclear decoupling in rotating solids, J. Chem. Phys. 103 (1995) 6951–6958.
[23] M. Kotecha, N.P. Wickramasinghe, Y. Ishii, Efficient low-power heteronuclear decoupling in ^{13}C high-resolution solid-state NMR under fast magic angle spinning, Magn. Reson. Chem. 45 (2007) S221–S230.
[24] I. Scholz, P. Hodgkinson, B.H. Meier, M. Ernst, Understanding two-pulse phase-modulated decoupling in solid-state NMR, J. Chem. Phys. 130 (2009) 114510.
[25] M. Weingarth, G. Bodenhausen, P. Tekely, Low-power decoupling at high spinning frequencies in high static fields, J. Magn. Reson. 199 (2009) 238–241.
[26] N.C. Nielsen, H. Bildsoe, H.J. Jakobsen, M.H. Levitt, Double-quantum homonuclear rotary resonance. Efficient dipolar recovery in magic-angle spinning nuclear magnetic resonance, J. Chem. Phys. 101 (1994) 1805–1812.
[27] C. Kehlet, T. Vosegaard, N. Khaneja, S.J. Glaser, N.C. Nielsen, Low-power homonuclear dipolar recoupling in solid-state NMR developed using optimal control theory, Chem. Phys. Lett. 414 (2005) 204–209.
[28] R. Verel, M. Baldus, M. Ernst, B.H. Meier, A homonuclear spin-pair filter for solid-state NMR based on adiabatic-passage techniques, Chem. Phys. Lett. 287 (1998) 421–428.
[29] R. Verel, M. Ernst, B.H. Meier, Adiabatic dipolar recoupling in solid-state NMR: the DREAM scheme, J. Magn. Reson. 150 (2001) 81–99.
[30] A.E. Bennett, J.H. Ok, R.G. Griffin, S. Vega, Chemical-shift correlation spectroscopy in rotating solids – radio frequency-driven dipolar recoupling and longitudinal exchange, J. Chem. Phys. 96 (1992) 8624–8627.
[31] M.J. Bayro, R. Ramachandran, M.A. Caporini, M.T. Eddy, R.G. Griffin, Radio frequency-driven recoupling at high magic-angle spinning frequencies: homonuclear recoupling sans heteronuclear decoupling, J. Chem. Phys. 128 (2008) 052321.
[32] M.J. Bayro, T. Maly, N.R. Birkett, C.M. Dobson, R.G. Griffin, Long-range correlations between aliphatic ^{13}C nuclei in protein MAS NMR spectroscopy, Angew. Chem.-Int. Ed. 48 (2009) 5708–5710.
[33] I. Scholz, M. Huber, T. Manolikas, B.H. Meier, M. Ernst, MIRROR recoupling and its application to spin diffusion under fast magic-angle spinning, Chem. Phys. Lett. 460 (2008) 278–283.
[34] M. Weingarth, D.E. Demco, G. Bodenhausen, P. Tekely, Improved magnetization transfer in solid-state NMR with fast magic angle spinning, Chem. Phys. Lett. 469 (2009) 342–348.
[35] G. De Paepe, J.R. Lewandowski, A. Loquet, A. Bockmann, R.G. Griffin, Proton assisted recoupling and protein structure determination, J. Chem. Phys. 129 (2008) 21.
[36] J.R. Lewandowski, G. De Paepe, M.T. Eddy, J. Struppe, W. Maas, R.G. Griffin, Proton assisted recoupling at high spinning frequencies, J. Phys. Chem. B 113 (2009) 9062–9069.
[37] S. Laage, A. Marchetti, J. Sein, R. Pierattelli, H.J. Sass, S. Grzesiek, A. Lesage, G. Pintacuda, L. Emsley, Band-selective $^{1}H—^{13}C$ cross-polarization in fast magic angle spinning solid-state NMR spectroscopy, J. Am. Chem. Soc. 130 (2008) 17216–17217.
[38] A. Lange, I. Scholz, T. Manolikas, M. Ernst, B.H. Meier, Low-power cross polarization in fast magic-angle spinning NMR experiments, Chem. Phys. Lett. 468 (2009) 100–105.
[39] J.R. Lewandowski, G. De Paepe, R.G. Griffin, Proton assisted insensitive nuclei cross polarization, J. Am. Chem. Soc. 129 (2007) 728–729.
[40] J.R. Lewandowski, G. De Paepe, M.T. Eddy, R.G. Griffin, $^{15}N—^{15}N$ proton assisted recoupling in magic angle spinning NMR, J. Am. Chem. Soc. 131 (2009) 5769–5776.
[41] I. Scholz, B.H. Meier, M. Ernst, NMR polarization transfer by second-order resonant recoupling: RESORT, Chem. Phys. Lett. 485 (2010) 335–342.
[42] K. Seidel, M. Etzkorn, H. Heise, S. Becker, M. Baldus, High-resolution solid-state NMR studies on uniformly [^{13}C, ^{15}N]-labeled ubiquitin, ChemBioChem 6 (2005) 1638–1647.
[43] G.A. Lazar, J.R. Desjarlais, T.M. Handel, De novo design of the hydrophobic core of ubiquitin, Protein Sci. 6 (1997) 1167–1178.
[44] R.W. Martin, K.W. Zilm, Preparation of protein nanocrystals and their characterization by solid state NMR, J. Magn. Reson. 165 (2003) 162–174.
[45] J.C. Hindman, Proton resonance shift of water in gas and liquid states, J. Chem. Phys. 44 (1966) 4582–4592.
[46] C.R. Morcombe, K.W. Zilm, Chemical shift referencing in MAS solid state NMR, J. Magn. Reson. 162 (2003) 479–486.
[47] W. Cochran, B.R. Penfold, The crystal structure of L-glutamine, Acta Crystallogr. 5 (1952) 644–653.
[48] A. Wagner, P. Luger, Charge density and topological analysis of L-glutamine, J. Mol. Struct. 595 (2001) 39–46.
[49] S.A. Smith, T.O. Levante, B.H. Meier, R.R. Ernst, Computer simulations in magnetic resonance. An object-oriented programming approach, J. Magn. Reson., Ser. A 106 (1994) 75–105.
[50] I. Scholz, B.H. Meier, M. Ernst, Operator-based triple-mode Floquet theory in solid-state NMR, J. Chem. Phys. 127 (2007) 204504.
[51] E.O. Stejskal, J. Schaefer, J.S. Waugh, Magic-angle spinning and polarization transfer in proton-enhanced NMR, J. Magn. Reson. 28 (1977) 105–112.
[52] M. Sardashti, G.E. Maciel, Effects of sample spinning on cross polarization, J. Magn. Reson. 72 (1987) 467–474.
[53] B.H. Meier, Cross polarization under fast magic angle spinning: thermodynamical considerations, Chem. Phys. Lett. 188 (1992) 201–207.
[54] S. Hediger, B.H. Meier, R.R. Ernst, Cross polarization under fast magic angle sample spinning using amplitude-modulated spin-lock sequences, Chem. Phys. Lett. 213 (1993) 627–635.
[55] R. Gonzalez-Mendez, H. Engeseth, A.A.B. Gibson, J. Deolivares, L. Litt, T.L. James, The modulation theorem in tailored radiofrequency excitation and its application to a notch filter, J. Magn. Reson. 78 (1988) 308–313.
[56] J. Boyd, N. Soffe, Selective excitation by pulse shaping combined with phase modulation, J. Magn. Reson. 85 (1989) 406–413.
[57] S.L. Patt, Single- and multiple-frequency-shifted laminar pulses, J. Magn. Reson. 96 (1992) 94–102.
[58] D. Artemov, Z.M. Bhujwalla, J.D. Glickson, Band-selective heteronuclear cross polarization in liquids, J. Magn. Reson., Ser. B 107 (1995) 286–288.
[59] W.R.C. Croasmun, M.K. Robert, Two-Dimensional NMR Spectroscopy: Applications for Chemists and Biochemists, John Wiley & Sons, 1994.
[60] G. Metz, X.L. Wu, S.O. Smith, Ramped-amplitude cross polarization in magic-angle-spinning NMR, J. Magn. Reson., Ser. A 110 (1994) 219–227.
[61] M. Wilhelm, H. Feng, U. Tracht, H.W. Spiess, 2D CP/MAS ^{13}C isotropic chemical shift correlation established by ^{1}H spin diffusion, Wallace Brey Symposium, Academic Press Inc., Gainesville, Florida, 1997. pp. 255–260.
[62] A. Lange, K. Seidel, L. Verdier, S. Luca, M. Baldus, Analysis of proton–proton transfer dynamics in rotating solids and their use for 3D structure determination, J. Am. Chem. Soc. 125 (2003) 12640–12648.
[63] J.P. Amoureux, B.W. Hu, J. Trebosc, Q. Wang, O. Lafon, F. Deng, Homonuclear dipolar decoupling schemes for fast MAS, Solid State Nucl. Magn. Reson. 35 (2009) 19–24.
[64] E. Salager, R.S. Stein, S. Steuernagel, A. Lesage, B. Elena, L. Emsley, Enhanced sensitivity in high-resolution ^{1}H solid-state NMR spectroscopy with DUMBO dipolar decoupling under ultra-fast MAS, Chem. Phys. Lett. 469 (2009) 336–341.
[65] S. Paul, R.S. Thakur, M. Goswami, A.C. Sauerwein, S. Mamone, M. Concistre, H. Forster, M.H. Levitt, P.K. Madhu, Supercycled homonuclear dipolar decoupling sequences in solid-state NMR, J. Magn. Reson. 197 (2009) 14–19.
[66] M. Leskes, P.K. Madhu, S. Vega, Why does PMLG proton decoupling work at 65 kHz MAS?, J Magn. Reson. 199 (2009) 208–213.
[67] K. Mao, M. Pruski, Homonuclear dipolar decoupling under fast MAS: resolution patterns and simple optimization strategy, Journal of Magnetic Resonance 203 (2010) 144–149.
[68] R.K. Harris, Brian E. Mann, NMR and the Periodic Table, Academic Press, London, 1978.